Title

Optimizing Ion Transport in Polyether-Based Electrolytes for Lithium Batteries

Journal

Macromolecules, 51(8)

ISSN

0024-9297

Authors

Zheng, Qi

Pesko, Danielle M

Savoie, Brett M

et al.

Publication Date

2018-04-24

DOI

10.1021/acs.macromol.7b02706

Peer reviewed

Macromolecules

Article

Cite This: Macromolecules 2018, 51, 2847−2858

Optimizing Ion Transport in Polyether-Based Electrolytes for Lithium Batteries

Qi Zheng,[†] Danielle M. Pesko,[‡,§] Brett M. Savoie,[#] Ksenia Timachova,[‡,§] Alexandra L. Hasan,[‡] Mackensie C. Smith,[‡,§] Thomas F. Miller, III,*[,⊥] Geoffrey W. Coates,*[,†] and Nitash P. Balsara*[,‡,§,∥]

[†]Department of Chemistry and Chemical Biology, Baker Laboratory, Cornell University, Ithaca, New York 14853, United States

[‡]Department of Chemical and Biomolecular Engineering, University of California, Berkeley, Berkeley, California 94720, United States

[§]Materials Science Division and [∥]Energy Storage and Distributed Resources Division, Lawrence Berkeley National Laboratory, Berkeley, California 94720, United States

[⊥]Division of Chemistry and Chemical Engineering, California Institute of Technology, Pasadena, California 91125, United States

[#]Charles D. Davidson School of Chemical Engineering, Purdue University, 480 Stadium Mall Drive, West Lafayette, Indiana 47906, United States

Supporting Information

ABSTRACT: We report on the synthesis of poly(diethylene oxide-*alt*-oxymethylene), P(2EO-MO), via cationic ring-opening polymerization of the cyclic ether monomer, 1,3,6-trioxocane. We use a combined experimental and computational approach to study ion transport in electrolytes comprising mixtures of P(2EO-MO) and lithium bis(trifluoromethanesulfonyl) imide (LiTFSI) salt. Mixtures of poly(ethylene oxide) (PEO) and LiTFSI are used as a baseline. The maximum ionic conductivities, σ, of P(2EO-MO) and PEO electrolytes at 90 °C are 1.1 × 10^{-3} and 1.5 × 10^{-3} S/cm, respectively. This difference is attributed to the T_g of P(2EO-MO)/LiTFSI (−12 °C), which is significantly higher than that of PEO/LiTFSI (−44 °C) at the same salt concentration. Self-diffusion coefficients measured using pulsed-field gradient NMR (PFG-NMR) show that both Li^+ and $TFSI^-$ ions diffuse more rapidly in PEO than in P(2EO-MO). However, the NMR-based cation transference number in P(2EO-MO) (0.36) is approximately twice that in PEO (0.19). The transference number measured by the steady-state current technique, $t_{+,ss}$, in P(2EO-MO) (0.20) is higher than in PEO (0.08) by a similar factor. We find that the product $\sigma t_{+,ss}$ is greater in P(2-EO-MO) electrolytes; thus, P(2EO-MO) is expected to sustain higher steady-state currents under dc polarization, making it a more efficacious electrolyte for battery applications. Molecular-level insight into the factors that govern ion transport in our electrolytes was obtained using MD simulations. These simulations show that the solvation structures around Li^+ are similar in both polymers. The same is true for $TFSI^-$. However, the density of Li^+ solvation sites in P(2EO-MO) is double that in PEO. We posit that this is responsible for the observed differences in the experimentally determined transport properties of P(2EO-MO) and PEO electrolytes.

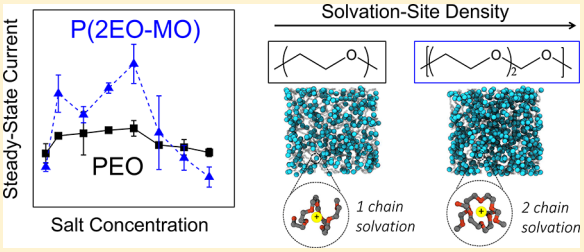

INTRODUCTION

Rechargeable lithium-ion batteries are an important component of the emerging clean energy landscape, currently being used in both electric vehicles and grid storage. There is considerable interest in finding a replacement for the flammable organic liquids used in conventional lithium-ion batteries. An electrolyte system that has garnered considerable interest is poly(ethylene oxide) (PEO) mixed with lithium salts. The solubility of alkali metal salts in PEO was first reported in the pioneering studies of Fenton, Parker, and Wright.[1] Since then, there have been significant advances in our understanding of the factors that affect the motion of Li^+ ions in polymer electrolytes. Spectroscopic studies and molecular dynamics (MD) simulations reveal that Li^+ is coordinated with ether oxygens on the polymer chain, indicating that ion motion is inherently coupled to polymer segmental motion.[2−9] A consequence of this coupling is that the ionic conductivity of polymer electrolytes is a strong function of the glass transition temperature, T_g, which governs segmental motion. Another important factor that affects ion transport is solvation-site connectivity.[10] This parameter is obtained from MD simulations by calculating the density of Li^+ solvation sites that occur naturally in a given polymer due to thermal fluctuations.

There have been numerous attempts to design and synthesize polymer electrolytes that are more efficacious than PEO.[11−37] In all of these studies, ion transport is characterized by measuring conductivity, σ, using ac impedance spectroscopy. It is, however, known that the performance of an electrolyte in rechargeable batteries depends on many more parameters.[38] In an important study, Bruce and Vincent conducted dc

Received: December 20, 2017
Revised: March 5, 2018
Published: April 3, 2018

DOI: 10.1021/acs.macromol.7b02706
Macromolecules 2018, 51, 2847−2858

experiments on polymer electrolytes using symmetric lithium−polymer−lithium cells.[39,40] They noted that in the dilute limit this approach gives the cation transference number. In concentrated electrolytes, however, the relationship between dc current in symmetric cells and the cation transference number is more complex.[41−43] Nevertheless, the apparent transference number measured using the approach of Bruce and Vincent, $t_{+,ss}$, is an important attribute of battery electrolytes. It is therefore not surprising that many papers on polymer electrolytes report $t_{+,ss}$.[44−50]

The performance of an electrolyte in a battery depends on its response to an applied dc potential. Predicting this response requires complete characterization of the electrolyte, i.e., knowledge of three transport parameters, σ, D, and t_+, where t_+ is the true transference number.[38] In the absence of complete characterization, the quantity that reflects the current obtained under an applied dc potential is the product $\sigma t_{+,ss}$. When the dc potential is initially applied, i.e., before concentration gradients have been established, the initial current, i_0, obtained through an electrolyte is given by Ohm's law

$$i_0 = \frac{\Delta V \sigma}{l} \tag{1}$$

where ΔV is the dc potential and l is the thickness of the electrolyte. The parameter $t_{+,ss}$ is defined as the fraction of the initial current that is sustained at steady state

$$t_{+,ss} = \frac{i_{ss}}{i_0} \tag{2}$$

where i_{ss} is the steady-state current. Thus, the product $\sigma t_{+,ss}$ is proportional to the steady-state current obtained through an electrolyte under a dc potential

$$\sigma t_{+,ss} = i_{ss}\left(\frac{l}{\Delta V}\right) \tag{3}$$

In this analysis, we restrict our attention to bulk (not interfacial) properties. In addition to the three transport parameters, interfacial impedance and exchange current densities will also affect electrolyte performance in a battery. However, these quantities are inherently dependent on the composition of the solid−electrolyte interface (SEI) layer and thus should be considered separately from bulk transport properties.

In this paper we report on the synthesis of a new polymer electrolyte, poly(diethylene oxide-*alt*-oxymethylene), referred to as P(2EO-MO). The monomer comprises two ethylene oxide moieties followed by a methylene oxide moiety, polymerized by ring-opening cationic polymerization. Previous studies of ethylene oxide-*co*-oxymethylene polymer electrolytes have focused mainly on cross-linked systems.[51−54] At least one study has reported on ion transport in a linear version of these copolymers; however, the conductivity measurements reported were limited to low temperatures.[55] Here, we characterize ion transport in mixtures of P(2EO-MO) and lithium bis(trifluoromethanesulfonyl) imide (LiTFSI) salt at 90 °C. We use transport measurements in PEO/LiTFSI electrolytes as a baseline for comparison. The chemical formulas of the polymers used in this study are shown in Figure 1. We demonstrate that $\sigma t_{+,ss}$ is larger in P(2EO-MO) than in PEO. Pulsed-field-gradient NMR (PFG-NMR) experiments are used to characterize the self-diffusion of ionic species in both electrolytes. Calculations of solvation-site connectivity and cation and anion self-diffusion coefficients using MD simulations provide some insight into the molecular underpinnings of our experimental observations.

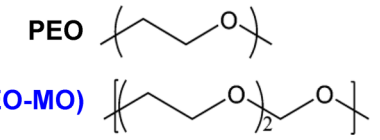

Figure 1. Structures for polymers used in this study.

EXPERIMENTAL SECTION

Polymer Synthesis. The synthesis of P(2EO-MO) has been previously reported.[56−58] Step-growth polymerization between diethylene glycol and paraformaldehyde results in the synthesis of an oligomer with a number-averaged molecular weight, M_n, of 1 kg/mol. The oligomer was heated to 150 °C under vacuum, depolymerized, and redistilled to yield the cyclic ether monomer, 1,3,6-trioxocane. P(2EO-MO) was synthesized using 2 mol % of $BF_3{\cdot}OEt_2$ as the initiator and dichloromethane (DCM) as the solvent at room temperature, as shown in Figure 2. The reaction, which was allowed

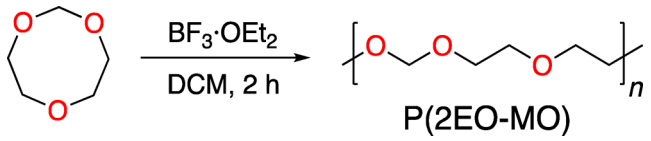

Figure 2. Synthesis of P(2EO-MO).

to proceed for 2 h, resulted in an equilibrium between high molecular weight polymer and oligo-macrocycles. The oligo-macrocycles were removed by precipitation in hexanes. The yielded polymer has an alternating sequence of MO and 2EO units, and no regio-defects are observed based on ^{13}C NMR; this alternating structure is caused by high reactivity of the acetal group in the monomer. The final M_n of the polymer was 55 kg/mol with a polydispersity index of 2.2, according to gel permeation chromatography (GPC). This chain length was significantly higher than that calculated based on the monomer-to-initiator ratio, suggesting that not all initiators participated in the polymerization. A similar discrepancy between experimental and theoretical M_ns has been reported by Chien and co-workers[56] in polymerizing 1,3,6-trioxocane in toluene with the $BF_3{\cdot}OEt_2$ catalyst. The Supporting Information contains a more rigorous description of the synthesis procedure, including NMR spectra and GPC traces of P(2EO-MO).

Electrolyte Preparation. The polymers used in this study are 100 kg/mol PEO, purchased from Sigma-Aldrich, and 55 kg/mol 2EO-MO, synthesized according to the procedure outlined in the Polymer Synthesis section. The conductivity[59,60] and Li^+ diffusivity[61] measured in PEO/LiTFSI mixtures have been shown to be independent of chain length above 5 kg/mol. Thus, we expect no significant difference in electrolyte properties to arise from the difference in M_n of our polymers.

Electrolytes were prepared by mixing polymer with lithium bis(trifluoromethanesulfonyl) imide (LiTFSI) salt purchased from Novolyte. All materials (PEO, P(2EO-MO), and LiTFSI) were thoroughly dried prior to use and maintained in an argon environment with H_2O and O_2 levels kept below 2 and 5 ppm, respectively. The polymers were dried at 90 °C under vacuum in the glovebox antechamber for 24 h. The salt was dried at 120 °C under vacuum in the glovebox antechamber for 3 days. Electrolytes were prepared by dissolving dry polymer and LiTFSI salt into tetrahydrofuran (THF) at 55 °C until completely dissolved. The THF was evaporated, leaving behind a homogeneous polymer/salt mixture. After 12 h of drying on the hot plate at 55 °C, the electrolytes were transferred to the glovebox antechamber to dry under vacuum at 90 °C for 24 h to remove any excess THF. The salt concentration in the electrolyte is described as r,

DOI: 10.1021/acs.macromol.7b02706
Macromolecules 2018, 51, 2847−2858

defined as the molar ratio of lithium ions to oxygen atoms on the polymer: $r = [Li^+]/[O]$. Electrolytes were prepared at r = 0.01, 0.02, 0.04, 0.06, 0.08, 0.10, 0.12, and 0.14 for each polymer.

Differential Scanning Calorimetry. Inside of a glovebox, each sample was prepared by depositing 2−5 mg of electrolyte into a hermetically sealed aluminum pan. Differential scanning calorimetry (DSC) was performed on each sample in a TA Instruments DSC Q200. The following temperature scan was used, beginning at room temperature: heat to 120 °C at 20 °C/min, cool to −90 °C at 5 °C/min, and heat to 120 °C at 20 °C/min. The resulting DSC curves of PEO and P(2EO-MO) electrolytes are shown in the Supporting Information. The glass transition temperature, T_g, and melting temperature, T_m, of each electrolyte were obtained from the second heating scan. Both measurements were reproducible within 1 °C.

Electrochemical Measurements. All electrochemical measurements were performed on a VMP3 potentiostat (Bio-Logic). For each measurement, data from three samples were averaged, and the error bars signify the standard deviation of these measurements.

Ac impedance spectroscopy was used to determine the ionic conductivity of the electrolytes. Stainless steel symmetric cells were prepared by pressing viscous electrolytes into a 3.175 mm diameter hole in a 508 μm thick silicone spacer, which was then pressed between two 200 μm thick stainless-steel shims used as electrodes. The electrolyte thickness was determined by measuring the total cell thickness using a micrometer and subtracting the thickness of the electrodes. Aluminum tabs were fastened to the electrodes using Kapton tape. The cell was hermetically sealed in Showa-Denko pouch material, leaving the tab ends exposed. This sample configuration allows for electrochemical measurements to take place outside of the glovebox while still maintaining an air- and water-free environment.

Once removed from the glovebox, each cell was placed in a custom-built heating stage to determine the ionic conductivity in the temperature range of 25−110 °C. Complex impedance measurements were taken with the frequency range of 1 Hz−1 MHz at an amplitude of 80 mV. The low-frequency minimum on the Nyquist impedance plot was taken to be the electrolyte bulk resistance, R_b, which was used along with electrolyte thickness, l, and electrolyte area, a, to calculate the electrolyte conductivity, σ, according to eq 4.

$$\sigma = \frac{l}{aR_b} \tag{4}$$

The inner diameter of the spacer, 3.175 mm, was used to calculate a. Thickness, l, was taken to be the final thickness of the electrolyte, measured after conductivity experiments were completed.

Steady-state current measurements were performed on lithium symmetric cells using a Biologic VMP3 potentiostat. A more detailed description of this experiment is provided in ref 42. Lithium symmetric cells were prepared by pressing electrolyte into a 508 μm thick silicone spacer and then sandwiching between two lithium electrodes (MTI corporation). Nickel tabs were used as electrical contacts. The assembly was vacuum sealed in a laminated aluminum pouch material (Showa-Denko) and then transferred to a heating stage at 90 °C for electrochemical measurements. Cells were annealed for 4 h then conditioned for five cycles at a low current density of 0.02 mA/cm^2 to introduce a stable interfacial layer. The cell was then polarized at constant potential, ΔV, for 4 h, and the steady-state current, i_{ss}, was recorded. Cell resistances were measured by performing ac impedance spectroscopy before polarization and during steady state. This experiment was repeated using ΔV = 10, −10, 20, and −20 mV, and the results were averaged to ensure that the ion transport characteristics were independent of the sign and magnitude of ΔV.

Ohm's law is used to determine current in the absence of concentration gradients

$$i_\Omega = \frac{\Delta V}{R_{i,0} + R_{b,0}} \tag{5}$$

where $R_{i,0}$ and $R_{b,0}$ are the interfacial and bulk electrolyte resistances measured prior to polarization. We use this approach to calculate the initial current, i_Ω, resulting from an applied potential, ΔV.

The steady-state current transference number defined by the work of Bruce and Vincent[39,40] is calculated using eq 6.

$$t_{+,ss} = \frac{i_{ss}(\Delta V - i_\Omega R_{i,0})}{i_\Omega(\Delta V - i_{ss}R_{i,ss})} \tag{6}$$

PFG-NMR Measurements. PFG-NMR was performed on PEO and P(2EO-MO) electrolytes with salt concentrations of r = 0.08 at temperatures of T = 60, 70, 80, and 90 °C for PEO and T = 90, 100, 110, and 120 °C for P(2EO-MO). NMR measurements were performed on a Bruker Avance 600 MHz instrument fitted with a Z-gradient direct detection broad-band probe and a variable temperature unit. Temperature was calibrated using the chemical shift separation of −OH resonances and $-CH_2-$ resonances of 20% ethylene glycol in dimethyl sulfoxide for the measurements performed between 60 and 120 °C. Diffusion measurements were performed on the isotopes of ^{7}Li and ^{19}F, which produced peaks around 233 and 565 MHz, respectively, to track the lithium- and fluorine-containing salt species. The 90° pulse lengths were optimized for each sample to achieve maximum signal amplitude. A stimulated echo bipolar gradient pulse sequence was used to measure the self-diffusion coefficients, D_i. The attenuation of the echo E was fit to eq 7

$$E = e^{-\gamma^2 g^2 \delta^2 D_i(\Delta - \delta/3)} \tag{7}$$

where γ is the gyromagnetic ratio, g is the gradient strength, δ is the duration of the gradient pulse, Δ is the interval between gradient pulses, and D_i is the self-diffusion coefficient. Diffusion time intervals were chosen based on appropriate signal decay and T_1 relaxation times. Parameters used for acquisition were diffusion intervals Δ = 0.4−0.5 s (^{7}Li) and 0.5 s (^{19}F) and pulse lengths = 10−40 ms (^{7}Li) and 5−10 ms (^{19}F). For each diffusion measurement, 32 experiments of varying gradient strength up to 0.33 T/m were performed, and the change in amplitude of the attenuated signal was fit to obtain the parameter D_i. All measured signal attenuations were single-exponential decays, and the errors in the fits were less than 2%.

Molecular Dynamics (MD) Simulations. All MD simulations were performed within the LAMMPS software suite.[62] All simulations utilized an adapted Trappe-UA force-field that has been reported previously[63] and employed periodic boundary conditions, particle−particle−particle−mesh (pppm) evaluations of long-range interactions beyond a 14 Å cutoff, a Nosé−Hoover barostat with 1000 fs relaxation, and a Nosé−Hoover thermostat with 100 fs relaxation (NPT). Equations of motion were evolved using the velocity-Verlet integrator and a 1 fs time step. Intramolecular Lennard-Jones interactions for atom pairs connected by fewer than four bonds were excluded during the MD simulations, and electrostatic 1−4 interactions were scaled by 0.5, conforming with Trappe-UA definitions.

Four separate trajectories were run for each polymer at each salt concentration. Each trajectory included a single polymer chain with a mass of approximately 20 kg/mol that was initialized using a protocol to randomize chain orientation and avoid configurations with significant overlap between atoms. Ions were added to random positions in each simulation box at a level consistent with the reported r values. The simulations were initially relaxed at constant NVE with constrained atom displacements of 0.1 Å for 10 ps, followed by five cycles of box compression/expansion between number densities of 0.045 and 0.09 atoms/Å^3 at 2000 K, with each compression/expansion being linearly applied over a 10 ps interval. The simulations were subsequently equilibrated at a temperature of 400 K and a pressure of 1 atm for 10 ns before running long-time scale production runs of 150 ns.

Diffusivities were calculated for each ion according to the Einstein equation

$$D_i = \lim_{t\to\infty} \frac{d\langle|\mathbf{r}_i(t) - \mathbf{r}_i(0)^2|\rangle}{6\,dt} \tag{8}$$

where D_i is the diffusion coefficient for ion, i, and the term in parentheses is the mean-squared displacement (MSD) evaluated at time t.

DOI: 10.1021/acs.macromol.7b02706
Macromolecules 2018, 51, 2847−2858

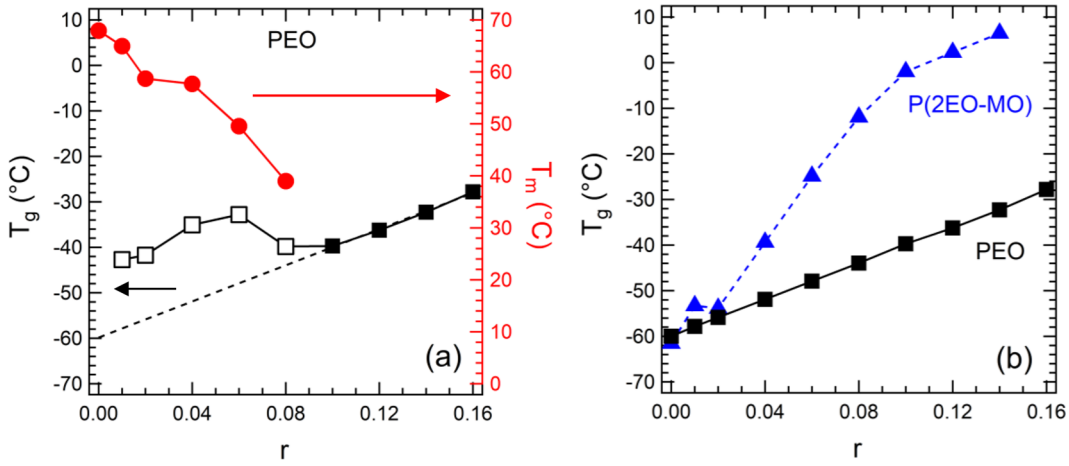

Figure 3. (a) Glass transition temperature (left axis) and melting temperature (right axis) of PEO/LiTFSI electrolytes. The black dotted line shows a linear fit of T_g from $r = 0.1$ to $r = 0.16$. (b) Glass transition temperature of PEO and P(2EO-MO) as a function of LiTFSI salt concentration.

Chemically Specific Dynamic Bond Percolation (CS-DBP) Simulations. CS-DBP is a methodology for calculating the long-time scale ion diffusivity using a coarse-grained description of ion hopping in terms of the ion solvation sites.[63] Here, we use the CS-DBP methodology to calculate and compare the Li^+ ion solvation site distributions in PEO and P(2EO-MO). Sites are generated via trial insertions of the ion into a previously equilibrated polymer simulation, followed by short trajectories to evaluate the stability of the solvation site. Specific details of the protocol can be found in ref 63. The prerequisite MD simulations for CS-DBP were initialized identically to the dilute concentration long-time scale MD simulations for the Li^+ ion, including four separate trajectories for each polymer. Each simulation was equilibrated for 10 ns at 400 K followed by an additional 10 ns trajectory that was used as an input for the CS-DBP site finding simulations. The reported site densities for each polymer reflect the average over four snapshots and reflect the outcome of approximately 5000 trial insertions of the Li^+ ion into each polymer.

RESULTS AND DISCUSSION

Electrolyte Characterization. DSC was performed on PEO/LiTFSI and P(2EO-MO)/LiTFSI electrolytes to investigate the effect of salt on the thermal properties of the polymer. Figure 3a shows the T_g and T_m obtained in PEO electrolytes as a function of salt concentration, r, where $r = [Li^+]/[O]$. We find that the T_m of PEO/LiTFSI decreases with increasing salt concentration up to $r = 0.08$; no T_m is observed from $r = 0.1$–0.16, indicating that PEO electrolytes in this regime are fully amorphous. DSC measurements of T_g in PEO/LiTFSI exhibit a nonmonotonic dependence on r, increasing from $r = 0.01$ to 0.06, decreasing from $r = 0.06$ to 0.1, and finally increasing from $r = 0.1$ to 0.16. For highly crystalline polymers, it has been suggested that segmental motion in the amorphous regions is restricted by the surrounding crystalline regions, and this leads to a measured T_g that is higher than what is representative of the bulk-amorphous phase.[64,65] We attribute the nonmonotonic dependence of T_g at $r \leq 0.08$ to this effect. The T_g of the amorphous phase in this regime is thus calculated by extrapolating the least-squares linear fit of the T_g measured in the amorphous electrolytes ($r \geq 0.1$). This fit is shown as the black dotted line in Figure 3 and is in the form of $T_g(r) = mr + b$, where $m = 198.9$ °C and $b = -59.9$ °C. Using this equation, we obtain a $T_g = -60$ °C for $r = 0$, which is in agreement with the T_g of neat PEO. Our approach for determining T_g at low salt concentrations is also consistent with observations in noncrystalline polyether-based electrolytes that exhibit a monotonic increase in T_g with increasing salt concentration.[10,12,17,30,34,51,66]

Figure 3b shows the T_g of P(2EO-MO)/LiTFSI electrolytes along with those obtained for PEO/LiTFSI using the analysis described above. We note that P(2EO-MO) electrolytes are noncrystalline above $r = 0.02$; thus, measured T_gs are presented in Figure 3b. Both polymers exhibit a T_g in the vicinity of −60 °C in the neat state. As r is increased, the T_gs of both electrolytes increase monotonically. This observation is commonly attributed to the physical cross-linking of the polymer chains mediated by solvated ions in the electrolyte. Interestingly, P(2EO-MO) exhibits a more dramatic increase in T_g with increasing r compared to PEO. This suggests fundamental differences in the mechanism of ion solvation in P(2EO-MO) and PEO electrolytes. In the following section, we use MD simulations to study the solvation of Li^+ and $TFSI^-$; these results provide insight into the concentration dependence of T_g in our electrolytes.

Ionic conductivity, σ, of PEO/LiTFSI and P(2EO-MO)/LiTFSI at 90 °C is shown as a function of r in Figure 4. Both electrolytes exhibit a nonmonotonic dependence on r, reaching

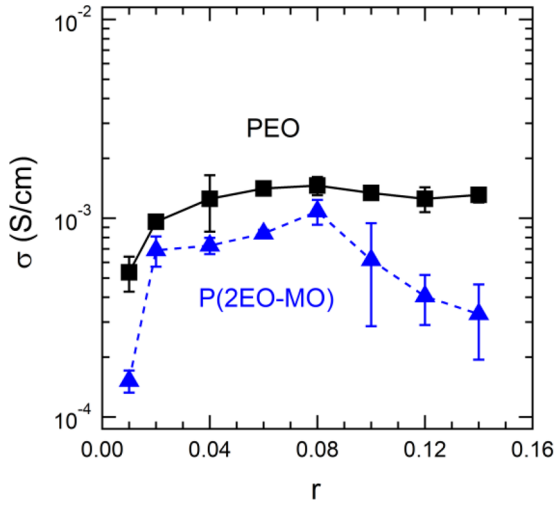

Figure 4. Ionic conductivity of PEO and P(2EO-MO) electrolytes as a function of LiTFSI salt concentration. These data are measured at 90 °C.

DOI: 10.1021/acs.macromol.7b02706
Macromolecules 2018, 51, 2847−2858

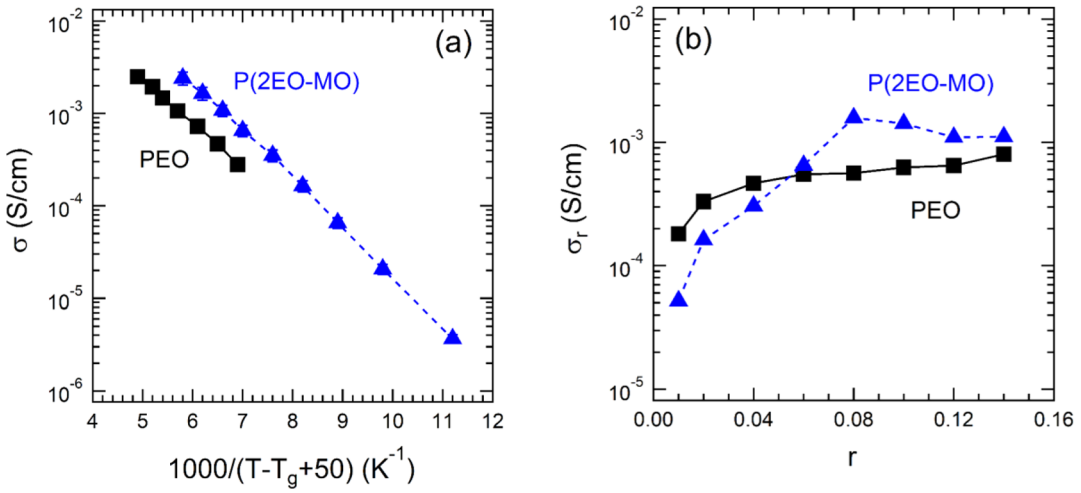

Figure 5. (a) Vogel–Tammann–Fulcher plot of conductivity at $r = 0.08$. (b) Reduced conductivity of PEO and P(2EO-MO) calculated according to eq 10, where $T = T_g + 110$ K or $1000/(T - T_g + 50) = 6.25$.

a maximum conductivity at $r = 0.08$. The maximum conductivity of PEO is 1.5×10^{-3} S/cm, while that of P(2EO-MO) is 1.1×10^{-3} S/cm. The conductivity of PEO remains above that of P(2EO-MO) for all salt concentrations in this study. This difference is especially significant at the most dilute salt concentration ($r = 0.01$) and in the highly concentrated regime ($r = 0.10$–0.14). The differences of PEO and P(2EO-MO) conductivity at high salt concentrations may be attributed to the differences in the glass transition temperatures, T_g, of the electrolytes. In simple electrolytes, one expects conductivity to increase linearly with salt concentration due to the increase in charge carrier concentration. In polymer electrolytes, ion transport is closely coupled to segmental relaxation of polymers,[61,67,68] which slows down with added salt due to associations between ions and the polymer segments. The trade-off between these two effects results in a conductivity maximum (e.g., Figure 4). The glass transition temperature is a simple measure of segmental relaxation. The T_g of P(2EO-MO) increases rapidly with salt concentration relative to PEO, resulting in a sharper conductivity peak. On the basis of the data in Figure 4, one might conclude that PEO/LiTFSI is a more efficacious battery electrolyte than P(2EO-MO)/LiTFSI. The discussion below critically examines this statement.

Conductivity is dependent on a number of factors including segmental motion of the polymer chains, the numbers of ions in the electrolyte, and the mobility of the ions. In an attempt to decouple the effect of segmental motion on conductivity, we use the Vogel–Tammann–Fulcher (VTF) equation[69]

$$\sigma = AT^{-1/2} \exp\left(\frac{-E_a}{R(T - T_0)}\right) \tag{9}$$

to fit our temperature-dependent conductivity data. In this equation, σ is expressed in terms VTF parameters, A and E_a, the universal gas constant, R, and the reference temperature, T_0. We take T_0 to be 50 °C below the concentration-dependent T_g of the electrolyte (Figure 4b), in accordance with previous literature.[70,71] In Figure 5a we plot σ versus $1000/(T - T_g + 50)$ for PEO and P(2EO-MO) at $r = 0.08$, the concentration at which both polymers experience a maximum conductivity. Here, we are only interested in observing the temperature dependence of fully amorphous electrolytes; we have thus excluded the data for PEO when $T \leq 40$ °C, the melting point of PEO/LiTFSI at $r = 0.08$. All temperatures for P(2EO-MO) are included, as this electrolyte has no detectable melting temperature. Both data sets are approximately linear, indicating good agreement with the VTF equation. Comparing conductivity at a set $T - T_g$, referred to as reduced temperature allows us to account for differences in T_g in P(2EO-MO) and PEO electrolytes. We find that the conductivity of P(2EO-MO) is higher than that of PEO at all values of $1000/(T - T_g + 50)$. Thus, differences in conductivity between these two polymers are not simply explained by differences in segmental motion, i.e., differences in T_g. Instead, our data suggest the mechanism of ion transport in P(2EO-MO) is fundamentally different from that of PEO.

To extend this analysis to all salt concentrations in our study, we calculate a reduced conductivity, σ_r, for each electrolyte at a fixed temperature (110 K) above the T_g of the electrolyte

$$\sigma_r = A(T_g + 110\ \text{K})^{-1/2} \exp\left(\frac{-E_a}{R(160\ \text{K})}\right) \tag{10}$$

Equation 10 is obtained by substituting $T = T_g + 110$ K in eq 9, where T_g is dependent on the salt concentration of the electrolyte (Figure 4b). The parameters A and E_a are obtained by least-squares fits through the temperature-dependent conductivity data; these values are given in Table 1. When compared at the same r, there is good agreement between E_a in PEO and P(2EO-MO) electrolytes, indicating that the VTF

Table 1. VTF Fit Parameters Obtained from a Least-Squares Fit to the Temperature-Dependent Conductivity Data of Each Electrolyte According to Eq 9

	PEO		P(2EO-MO)	
r	E_a (kJ/mol)	A (S K$^{1/2}$/cm)	E_a (kJ/mol)	A (S K$^{1/2}$/cm)
0.01	7.8	1.1	9.0	0.8
0.02	8.1	2.6	10.7	9.4
0.04	8.4	4.6	9.4	6.9
0.06	8.7	7.1	10.4	29.6
0.08	9.9	18.4	10.2	65.4
0.10	9.2	11.6	9.9	47.1
0.12	9.2	12.2	8.9	17.4
0.14	9.1	13.8	8.7	15.1

DOI: 10.1021/acs.macromol.7b02706
Macromolecules 2018, 51, 2847–2858

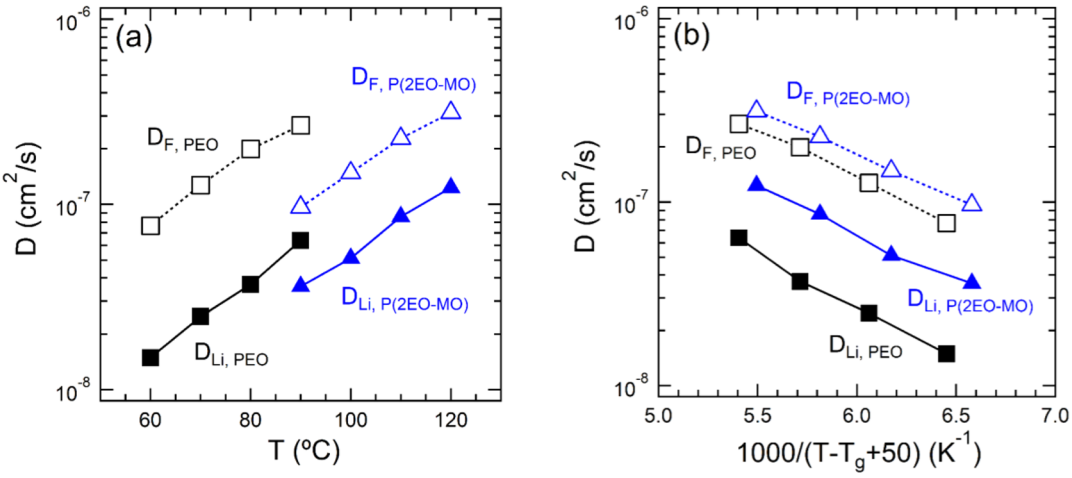

Figure 6. (a) Self-diffusion coefficients of lithium- and fluorine-containing species in PEO and P(2EO-MO) at r = 0.08. (b) Same data plotted as a function of reduced temperature.

lines are nearly parallel (Figure 5a). Thus, our choice of 110 K as the reduced temperature is arbitrary; any value of $T - T_g$ would lead to a qualitatively similar dependence of σ_r on r. Figure 5b shows σ_r in PEO and P(2EO-MO) electrolytes as a function of r. At low salt concentrations ($r < 0.06$) PEO has a higher reduced conductivity compared to that of P(2EO-MO), while above r = 0.06 σ_r in P(2EO-MO) electrolytes surpasses that of PEO. Reduced conductivity has been studied for a number of different electrolytes,[10,60,72,68] and P(2EO-MO)/LiTFSI is the first system to exhibit a σ_r greater than that of PEO/LiTFSI. A greater reduced conductivity could be attributed to improved lithium mobility, improved anion mobility, or a larger degree of dissociation between ions, leading to a greater number of effective charge carriers in the system. More information is required to identify which case applies to P(2EO-MO) electrolytes at high salt concentrations.

Self-diffusion coefficients of the lithium- and fluorine-containing species (D_{Li} and D_F) were measured using ^{7}Li and ^{19}F pulsed-field gradient NMR (PFG-NMR). If the salt were fully dissociated, then D_{Li} would reflect the self-diffusion of the cation while D_F would reflect the self-diffusion of the anion. Figure 6a shows D_{Li} and D_F for PEO/LiTFSI and P(2EO-MO)/LiTFSI electrolytes at r = 0.08. In both polymers, D_F is greater than D_{Li}, suggesting the anion is diffusing faster than the cation at a given temperature. This finding is consistent with previous reports of PFG-NMR of PEO electrolytes.[73−77] The slow diffusion of Li^+ is often attributed to the strong interactions with the oxygens on the polymer, whereas the anion moves freely. We find both D_F and D_{Li} are greater in PEO than in P(2EO-MO), likely due to the higher T_g of P(2EO-MO) (−12 °C) compared to that of PEO (−44 °C) at r = 0.08. The T_g of an electrolyte is related to segmental motion; slow segmental motion often leads to slow ion diffusion, as seen in P(2EO-MO).

Following the same approach used in the conductivity analysis, we decouple the effect of segmental motion on D_{Li} and D_F using the diffusivity form of the VTF equation

$$D_i = BT^{1/2} \exp\left(\frac{-E_a}{R(T - T_0)}\right) \quad (11)$$

where all parameters are introduced in eq 9 apart from B, the VTF parameter for diffusivity, analogous to A in eq 9. The values of B and E_a obtained by least-squares fits of the diffusivity data are given in Table 2. The E_a values obtained from diffusivity reported in Table 2 are in agreement with those determined from conductivity reported in Table 1. Figure 5b shows D_{Li} and D_F versus reduced temperature for both polymers at r = 0.08. When differences in T_g are accounted for, D_F in PEO and P(2EO-MO) are comparable. Thus, the diffusion coefficient of the anion is mainly governed by the T_g of the electrolyte and is not strongly dependent on the chemistry of the monomer. On the other hand, even when differences in segmental motion are accounted for, D_{Li} in P(2EO-MO) remains above that of PEO (Figure 6b). Faster Li^+ diffusivity may be attributed to either (1) an increase in solvation-site density which increases the rate of hopping between solvation sites or (2) a difference in the solvation environment of the ion which results in weaker ion-polymer interactions. In discussions below, we use simulations to address this issue.

Table 2. VTF Fit Parameters Obtained from a Least-Squares Fit to the Temperature-Dependent Diffusivity Data for Both Electrolytes According to Eq 11

	PEO		P(2EO-MO)	
	E_a (kJ/mol)	B (cm^2/(K$^{1/2}$ s))	E_a (kJ/mol)	B (cm^2/(K$^{1/2}$ s))
D_{Li}	11.0	4.0×10^{-6}	9.3	2.9×10^{-6}
D_F	9.7	7.9×10^{-6}	8.8	5.4×10^{-6}

Using the parameters given in Table 2, we calculate a reduced self-diffusion coefficient, $D_{r,i}$, for each electrolyte where the temperature is defined to be 110 K above the T_g of the electrolyte.

$$D_{r,i} = B(T_g + 110\ \text{K})^{1/2} \exp\left(\frac{-E_a}{R(160\ \text{K})}\right) \quad (12)$$

In PEO $D_{r,Li} = 1.9 \times 10^{-8}$ cm^2/s and $D_{r,F} = 1.0 \times 10^{-7}$ cm^2/s, while in P(2EO-MO) $D_{r,Li} = 5.1 \times 10^{-8}$ cm^2/s and $D_{r,F} = 1.4 \times 10^{-7}$ cm^2/s. The differences in $D_{r,Li}$ provide insight into the observation that reduced conductivity of P(2EO-MO) is higher than that of PEO at r = 0.08 (Figure 5b).

DOI: 10.1021/acs.macromol.7b02706
Macromolecules 2018, 51, 2847−2858

Using the self-diffusion coefficients measured at 90 °C (Figure 6a), we can calculate the transference number obtained by PFG-NMR using eq 13.

$$t_{+,\mathrm{NMR}} = \frac{D_{\mathrm{Li}}}{D_{\mathrm{Li}} + D_{\mathrm{F}}} \tag{13}$$

We find that $t_{+,\mathrm{NMR}}$ in PEO is 0.19 while $t_{+,\mathrm{NMR}}$ in P(2EO-MO) is 0.36.

The transference number obtained from the steady-state current technique, $t_{+,ss}$, measured at 90 °C is shown as a function of r in Figure 7. The $t_{+,ss}$ of both PEO and P(2EO-MO) electrolytes decreases with increasing salt concentration: P(2EO-MO) has a local minima at r = 0.04 while PEO decreases monotonically. The $t_{+,ss}$ of P(2EO-MO) is approximately double that of PEO at all values of r in this study. This finding is consistent with our measurements of $t_{+,\mathrm{NMR}}$ in P(2EO-MO), which was also found to be twice that of PEO. The value of $t_{+,ss}$ is lower than that of $t_{+,\mathrm{NMR}}$ in both electrolyte systems, consistent with previous reports of these quantities in PEO electrolytes.[42,76−78] The fact that $t_{+,ss}$ and $t_{+,\mathrm{NMR}}$ differ substantially from each other indicates that ion dissociation in our electrolytes is complex. We note that $t_{+,ss}$ nor $t_{+,\mathrm{NMR}}$ should be interpreted as approximations of the true transference number; only in the dilute limit wherein ion-pairing and ion-clustering are absent, the transference numbers determined by the steady-state current method and NMR would be identical to the true transference number.[41−43]

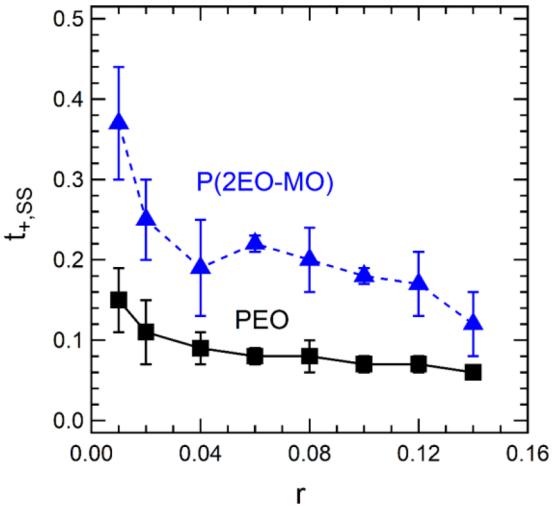

Figure 7. Transference number obtained using the steady-state for PEO and P(2EO-MO) as a function of LiTFSI salt concentration. These data are measured at 90 °C.

A simple measure of the efficacy of a polymer electrolyte is the product $\sigma t_{+,ss}$. This metric has been reported previously for PEO[78] as well as newly designed polymer electrolyte systems.[49,79] Figure 8 shows $\sigma t_{+,ss}$ as a function of salt concentration in PEO and P(2EO-MO) electrolytes. We find that P(2EO-MO) exhibits a $\sigma t_{+,ss}$ that is higher than PEO from r = 0.02 to r = 0.1. In this regime of salt concentration, P(2EO-MO) is expected to sustain higher steady-state currents in battery applications.

Molecular Dynamics and Coarse-Grained Simulations. Molecular dynamics (MD) simulations were used to shed light on the molecular origin of the experimental observations described above. Both PEO and P(2EO-MO) electrolytes were studied at r = 0.002, 0.01, 0.02, and 0.06. In addition, the dilute electrolyte was examined by considering a single anion or cation in the simulation box. All simulations were performed at 400 K using a previously reported simulation protocol.[10,63]

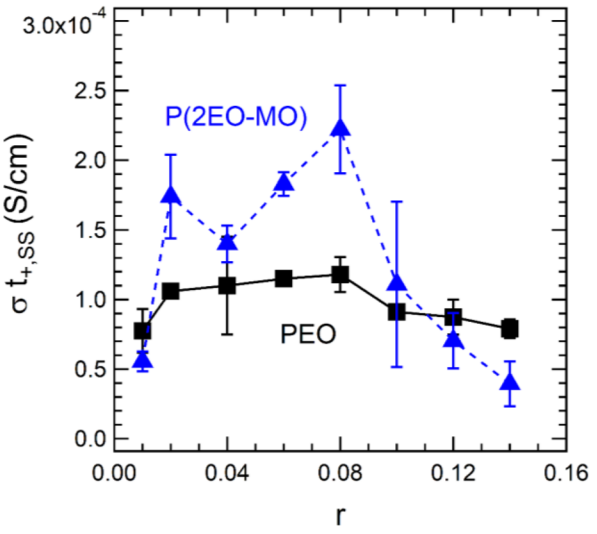

Figure 8. Product of conductivity (Figure 4a) and steady-state current transference number (Figure 7) as a function of LiTFSI salt concentration at 90 °C.

These simulations were used to characterize the solvation environment of Li^+ and $TFSI^-$ ions in our electrolytes. The radial distribution functions (rdfs) $g_{\mathrm{Li-O}}(r)$ and $g_{\mathrm{N-Li,C}}(r)$ were parsed from each simulation where "O" includes both the polymer and anion oxygens, "N" is the anion nitrogen atoms, "C" corresponds to the CH_2 united atoms, and "Li" is the lithium ions. In the dilute systems, the labels "O" and "C" refer exclusively to the polymer ether oxygens and CH_2 united atoms, respectively. The radial distribution functions were calculated according to eq 14

$$g_{\alpha-\beta}(r) = \frac{V}{4\pi r^2 \mathrm{d}r N_\alpha N_\beta} \sum_{i\in\alpha}^{N_\alpha} \sum_{j\in\beta}^{N_\beta} \delta(r - |\mathbf{r}_i - \mathbf{r}_j|) \tag{14}$$

where V is the volume of the simulation, N_α and N_β are the number of particles in each set, $4\pi r^2 \mathrm{d}r$ is the volume in each shell, $\mathbf{r}$ is the position of each atom, and the summations run separately over the two sets of atoms. Each rdf in was parsed from 50 ns of trajectory data, using frames spaced by 100 ps.

The Li^+ solvation structures in PEO and P(2EO-MO) electrolytes are characterized using $g_{\mathrm{Li-O}}$ (Figure 9a), which gives the radial distribution of oxygens surrounding the lithium ion. The electrolytes exhibit similar Li^+ solvation structures that are independent of salt concentration. In both PEO and P(2EO-MO), Li^+ is surrounded by six oxygen atoms in the first solvation shell, represented by a strong peak at 2 Å. The agreement between the dilute and concentrated electrolytes indicates that Li^+ solvation is dominated by oxygens on the polymer; there is minimal anion presence in the first solvation shell, suggesting weak ion pairing in both systems. The main difference between our two polymers is that the 2 Å peak in $g_{\mathrm{Li-O}}$ of P(2EO-MO) is slightly broader, resulting in a smaller peak height. Thus, the oxygens in the P(2EO-MO) solvation shell are slightly more distributed in terms of distance from Li^+. The significance of this observation is unknown. These solvation structures can be visualized in Figure 9b, which

DOI: 10.1021/acs.macromol.7b02706
Macromolecules 2018, 51, 2847−2858

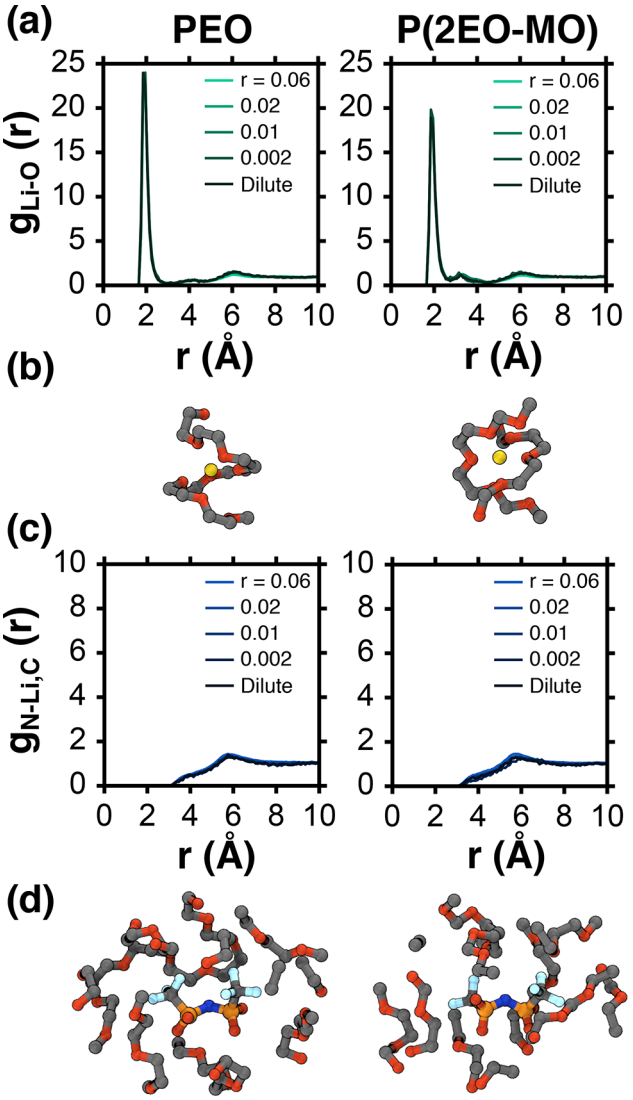

Figure 9. Comparison of ion solvation structures in PEO (left) and P(2EO-MO) (right). (a) Li^+ radial distribution functions at different salt concentrations. (b) Representative solvation structures for Li^+ in dilute electrolytes. (c) $TFSI^-$ radial distribution functions at different salt concentrations. (d) Representative solvation structures for $TFSI^-$ in dilute electrolytes. Atoms within 5 Å of Li^+ and 6 Å of nitrogen, sulfur, or fluorine are shown in the solvation structures of Li^+ and $TFSI^-$, respectively. Note: "*r*" in each legend refers to the salt concentration.

displays snapshots of typical solvation environments of Li^+ in dilute electrolytes. One notable difference in the two polymers is that two-chain solvation structures predominate in P(2EO-MO), whereas a majority of one-chain solvation structures are observed in PEO.[80] The reason for the two-chain motif in P(2EO-MO) is clearly the structure of the monomer: the presence of two oxygen atoms separated by a single methylene unit is inconsistent with the spacing requirements of typical solvation of Li^+ by ether oxygens. This precludes the possibility of solvating the ion with oxygens from one chain as is the case with PEO. We posit that the two-chain motif is responsible for the rapid increase seen in the experimentally measured T_g in P(2EO-MO)/LiTFSI with increasing salt concentration, relative to PEO (Figure 3b).

The $TFSI^-$ environment is examined in Figure 9c, which shows $g_{N-Li,C}$ for PEO and P(2EO-MO). These distribution functions are characterized by one weak shoulder at 6 Å corresponding to 10−12 weakly associated CH_2 groups. The fact that g_{Li-O} and $g_{N-Li,C}$ are identical in dilute and concentrated electrolytes indicates that both Li^+ and $TFSI^-$ are surrounded primarily by polymer chains; the ions are well dissociated in both systems. This is confirmed by Li-TFSI rdf provided in the Supporting Information. Typical solvation structures for the $TFSI^-$ ion are shown in Figure 9d. The arrangements of polymer chains around the central $TFSI^-$ ion are more or less random for both electrolytes.

Next, we calculate the Li^+ solvation-site density, ρ_{Li}, in both polymers; ρ_{Li} is the number of solvation sites per unit volume, as defined in ref 10. The solvation-site distributions are generated using the chemically specific bond percolation (CS-DBP) methodology by analyzing the nascent Li^+ solvation sites that are transiently formed during polymer fluctuations.[63] Figure 10 shows the solvation sites in PEO and P(2EO-MO) at

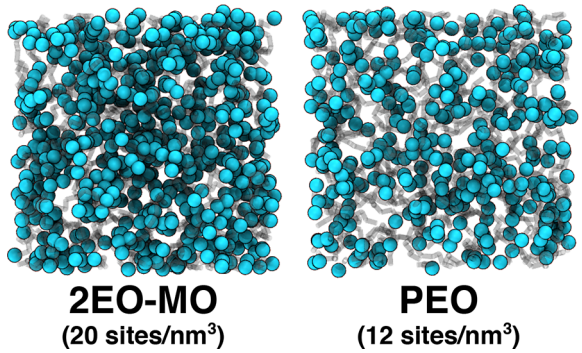

Figure 10. Comparison of CS-DBP solvation-site densities at 400 K.

a simulation temperature of 400 K (equilibration is challenging at lower temperatures). P(2EO-MO) exhibits approximately a 2-fold increase in ρ_{Li} (20 sites/nm^3) relative to PEO (12 sites/nm^3). Differences in ion transport properties (conductivity, diffusivity, and transference number) in PEO and P(2EO-MO) will be affected by differences in solvation-site density. In particular, the increase in solvation-site density is consistent with the experimentally observed increase in $D_{r,Li}$ and σ_r; holding other factors constant, increased ρ_{Li} has been found to correlate with increased Li^+ transport.[10]

The self-diffusion coefficients of both Li^+ and $TFSI^-$ in electrolytes were determined from all-atom MD simulations described in the context of Figure 9. The coefficients are obtained from the mean-squared displacements of each ion. At the two salt concentrations studied (r = 0.02 and r = 0.06), both Li^+ and $TFSI^-$ diffusivities are suppressed in P(2EO-MO) relative to PEO by approximately a factor of 2. For example, at r = 0.06, in P(2EO-MO) Li^+ diffusivity is 8.15×10^{-8} cm^2/s while $TFSI^-$ diffusivity is 4.89×10^{-7} cm^2/s, leading to $t_{+,MD}$ = 0.14. In PEO at r = 0.06, Li^+ diffusivity is 1.26×10^{-7} cm^2/s while $TFSI^-$ diffusivity is 9.23×10^{-7} cm^2/s, leading to $t_{+,MD}$ = 0.12. This is also observed experimentally. The cation transference numbers determined by MD simulations are likewise qualitatively consistent with the NMR measurements.

CONCLUSIONS

In this study, we report on the synthesis and characterization of a new polymer electrolyte, P(2EO-MO). Our characterization work includes both experimental and computational techniques. P(2EO-MO) was synthesized using cationic ring-opening

DOI: 10.1021/acs.macromol.7b02706
Macromolecules 2018, 51, 2847−2858

Table 3. Summary of Parameters Obtained in This Study for PEO and P(2EO-MO). Experimental Measurements Are for Electrolytes at r = 0.08 and T = 90°C. MD Simulations Were Performed at r = 0.06, and ρ_{Li} Was Determined in Dilute Electrolytes. for Each Column, P(2EO-MO)/PEO (Row 3) Gives the Ratio of the P(2EO-MO) Value (Row 1) to the PEO Value (Row 2)

	experiment							simulations			
	T_g (°C)	σ (S/cm)	D_{Li} (cm^2/s)	D_F (cm^2/s)	$t_{+,NMR}$	$t_{+,ss}$	$\sigma t_{+,ss}$ (S/cm)	ρ_{Li} (nm^{-3})	D_{Li} (cm^2/s)	D_F (cm^2/s)	$t_{+,MD}$
P(2EO-MO)	−12	1.1×10^{-3}	3.8×10^{-8}	9.7×10^{-8}	0.36	0.20	2.2×10^{-4}	20	8.2×10^{-8}	4.9×10^{-7}	0.14
PEO	−44	1.5×10^{-3}	6.4×10^{-8}	2.7×10^{-7}	0.19	0.08	1.2×10^{-4}	12	1.3×10^{-7}	9.2×10^{-7}	0.12
P(2EO-MO)/PEO		0.73	0.59	0.36	1.89	2.50	1.83	1.67	0.63	0.53	1.17

polymerization of the cyclic ether monomer, 1,3,6-trioxocane. Electrolytes were prepared by mixing P(2EO-MO) with lithium bis(trifluoromethanesulfonyl) imide (LiTFSI) salt at a wide range of salt concentrations, r = 0.01−0.14, where r = [Li$^+$]/[O]. We use the PEO/LiTFSI system as a baseline. The ion transport characteristics of the two electrolytes of interest are compared in Table 3.

Table 3 contains a summary of the experimental results for PEO and P(2EO-MO) electrolytes at r = 0.08. DSC measurements of both polymers exhibit T_gs in the vicinity of −60 °C in the neat state; P(2EO-MO), however, has a much more precipitous increase in T_g with salt concentration. For example, at r = 0.08 the T_g of P(2EO-MO)/LiTFSI (−12 °C) is significantly higher than that of PEO/LiTFSI (−44 °C) at the same salt concentration (Table 3). The conductivity of our electrolytes is affected by T_g. The σ of PEO at 90 °C is 1.5×10^{-3} S/cm while that of P(2EO-MO) is 1.1×10^{-3} S/cm. To gain an understanding of transport of individual ions in these systems, we used PFG-NMR to measure the self-diffusion coefficients of Li- and F-containing ions in our electrolytes. Table 3 shows that both ions exhibit higher diffusivity in PEO. Based on this set of information, most studies would conclude that PEO is the superior choice for a battery electrolyte. However, more complete characterization indicates that this is not true. Transference number measurements using the steady-state current technique show that P(2EO-MO) has a $t_{+,ss}$ that is approximately double that of PEO. This is qualitatively consistent with the transference number determined from PFG-NMR (Table 3). The steady-state dc current obtained in an electrolyte is governed by the product $\sigma t_{+,ss}$, which is higher in P(2EO-MO) compared to PEO. In other words, batteries made with P(2EO-MO) electrolytes are expected to be more efficacious compared to those made with PEO. We hope to demonstrate this in future studies.

Atomistic MD simulations were used to analyze the solvation structure of the Li$^+$ and TFSI$^-$ ions in PEO and P(2EO-MO) for a range of r; results confirmed that differences in transport properties could not be attributed to differences in solvation structure. The main difference is that P(2EO-MO) preferentially solvates Li$^+$ using a two-chain solvation motif, whereas PEO has contributions of both one-chain and two-chain solvation. The consequence of this two-chain solvation in P(2EO-MO) may be the rapid increase in T_g with salt concentration. The density of Li$^+$ solvation sites, ρ_{Li}, calculated from simulations was higher in P(2EO-MO) relative to PEO (Table 3). We posit that differences in experimentally determined ion transport properties in the two electrolytes are primarily due to this effect. The diffusion coefficients of Li$^+$ and TFSI$^-$ obtained using simulations are qualitatively consistent with experimental data. The simulations do capture the fact that the transference number of P(2EO-MO) electrolytes is higher than that of PEO electrolytes.

The ratio of transport properties of the two polymers of interest are also reported in Table 3. We see that conductivity and diffusion coefficients (in both experiments and simulations) are affected by T_g; transport parameters in P(2EO-MO) are lower than those in PEO, and all the ratios are less than unity. On the other hand, the transference numbers determined by NMR, electrochemical methods, and MD simulations appear to be governed by factors other than T_g, as they are greater in P(2EO-MO). The same can be said for solvation-site density.

Our work demonstrates that the discovery of new electrolytes is facilitated by the use of complementary experimental and theoretical approaches.

■ ASSOCIATED CONTENT

Supporting Information

The Supporting Information is available free of charge on the ACS Publications website at DOI: 10.1021/acs.macromol.7b02706.

Synthesis details including monomer synthesis, polymerization procedure, GPC traces, and NMR spectra of P(2EO-MO); DSC traces of PEO and P(2EO-MO) electrolytes; Li-TFSI radial distribution functions from MD simulations (PDF)

■ AUTHOR INFORMATION

Corresponding Authors

*E-mail: nbalsara@berkeley.edu (N.P.B.).
*E-mail: gc39@cornell.edu (G.W.C.).
*E-mail: tfm@caltech.edu (T.F.M.III).

ORCID

Danielle M. Pesko: 0000-0002-4833-0119
Ksenia Timachova: 0000-0001-8200-3552
Thomas F. Miller III: 0000-0002-1882-5380
Geoffrey W. Coates: 0000-0002-3400-2552
Nitash P. Balsara: 0000-0002-0106-5565

Author Contributions

Q.Z. and D.M.P. contributed equally to the work.

Notes

The authors declare no competing financial interest.

■ ACKNOWLEDGMENTS

The authors gratefully acknowledge Zhen-Gang Wang and Michael Webb for useful discussions. This research was supported by the National Science Foundation under DMREF Award NSF-CHE-1335486. DSC experiments were performed at the Molecular Foundry user facilities at Lawrence Berkeley National Laboratory supported by the Office of Science, Office of Basic Energy Sciences, of the U.S. Department of Energy under Contract DE-AC02-05CH11231.

DOI: 10.1021/acs.macromol.7b02706
Macromolecules 2018, 51, 2847−2858

■ ABBREVIATIONS

PEO	poly(ethylene oxide)
P(2EO-MO)	poly(diethylene oxide-*alt*-oxymethylene)
LiTFSI	lithium bis(trifluoromethanesulfonyl)imide
SEI	solid−electrolyte interface
NMR	nuclear magnetic resonance spectroscopy
PFG-NMR	pulsed-field-gradient NMR
GPC	gel permeation chromatography
DCM	dichloromethane
THF	tetrahydrofuran
DSC	differential scanning calorimetry
pppm	particle−particle−particle−mesh
MSD	mean-squared displacement
CS-DBP	chemically specific dynamic bond percolation
rdf	radial distribution function
T_g	glass transition temperature (°C)
T_m	melting temperature (°C)
M_n	number-averaged molecular weight (kg/mol)
σ	conductivity (S/cm)
σ_r	reduced conductivity (S/cm)
D	salt diffusion coefficient (cm^2/s)
D_i	self-diffusion coefficient (cm^2/s)
D_{Li}	lithium self-diffusion coefficient (cm^2/s)
D_F	fluorine self-diffusion coefficient (cm^2/s)
$D_{r,i}$	reduced self-diffusion coefficient (cm^2/s)
$D_{r,Li}$	reduced lithium self-diffusion coefficient (cm^2/s)
$D_{r,F}$	reduced fluorine self-diffusion coefficient (cm^2/s)
t_+	true cation transference number
$t_{+,ss}$	transference number obtained using stead-state current method
$t_{+,NMR}$	transference number obtained using pulsed-field gradient NMR
$t_{+,MD}$	transference number obtained using MD simulations
i_0	initial current (mA/cm^2)
i_Ω	initial current determined by Ohm's law (mA/cm^2)
i_{ss}	steady-state current (mA/cm^2)
ΔV	dc potential (mV)
R_b	bulk electrolyte resistance ($\Omega\ cm^2$)
$R_{i,0}$	initial interfacial resistance ($\Omega\ cm^2$)
$R_{b,0}$	initial bulk electrolyte resistance ($\Omega\ cm^2$)
r	moles of Li^+ per mole of ether oxygens
l	electrolyte thickness (cm)
a	electrolyte area (cm^2)
t	time (s)
T	temperature (°C)
E	attenuation of the echo
γ	gyromagnetic ratio
δ	duration of gradient pulse (s)
Δ	interval between gradient pulses (s)
T_0	reference temperature (°C)
A	VTF prefactor for conductivity ($S\ K^{1/2}/cm$)
B	VTF prefactor for diffusivity ($cm^2/(s\ K^{1/2})$)
E_a	effective activation energy (kJ/mol)
R	universal gas constant (kJ/(mol K))
g_{Li-O}	lithium−oxygen radial distribution function
$g_{N-Li,C}$	nitrogen−lithium,carbon radial distribution function
r_i	position of the atom (Å)
V	volume of the simulation cell (nm^3)
N_α	number of particles in α
N_β	number of particles in β
ρ_{Li}	Li^+ solvation-site density (nm^{-3})

■ REFERENCES

(1) Fenton, D. E.; Parker, J. M.; Wright, P. V. Complexes of alkali metal ions with poly(ethylene oxide). *Polymer* **1973**, *14*, 589.

(2) Papke, B. L.; Ratner, M. A.; Shriver, D. F. Vibrational Spectroscopic Determination of Structure and Ion Pairing in Complexes of Poly(ethylene oxide) with Lithium Salts. *J. Electrochem. Soc.* **1982**, *129*, 1434.

(3) Mao, G.; Saboungi, M.-L.; Price, D. L.; Badyal, Y. S.; Fischer, H. E. Lithium environment in PEO-$LiClO_4$ polymer electrolyte. *Europhys. Lett.* **2001**, *54*, 347−353.

(4) Wen, S. J.; Richardson, T. J.; Ghantous, D. I.; Striebel, K. A.; Ross, P. N.; Cairns, E. J. FTIR characterization of PEO + LiN(CF3SO2)2 electrolytes. *J. Electroanal. Chem.* **1996**, *408*, 113−118.

(5) Rey, I.; Lassègues, J. C.; Grondin, J.; Servant, L. Infrared and Raman study of the PEO-LiTFSI polymer electrolyte. *Electrochim. Acta* **1998**, *43*, 1505−1510.

(6) Mao, G.; Saboungi, M.-L.; Price, D. L.; Armand, M. B.; Howells, W. S. Structure of Liquid PEO-LiTFSI Electrolyte. *Phys. Rev. Lett.* **2000**, *84*, 5536−5539.

(7) Borodin, O.; Smith, G. D. Mechanism of ion transport in amorphous poly(ethylene oxide)/LiTFSI from molecular dynamics simulations. *Macromolecules* **2006**, *39*, 1620−1629.

(8) Müller-Plathe, F.; van Gunsteren, W. F. Computer simulation of a polymer electrolyte: Lithium iodide in amorphous poly(ethylene oxide). *J. Chem. Phys.* **1995**, *103*, 4745−4756.

(9) Diddens, D.; Heuer, A.; Borodin, O. Understanding the Lithium Transport within a Rouse-Based Model for a PEO/LiTFSI Polymer Electrolyte. *Macromolecules* **2010**, *43*, 2028−2036.

(10) Pesko, D. M.; Webb, M. A.; Jung, Y.; Zheng, Q.; Miller, T. F., III; Coates, G. W.; Balsara, N. P. Universal Relationship between Conductivity and Solvation-Site Connectivity in Ether-Based Polymer Electrolytes. *Macromolecules* **2016**, *49*, 5244−5255.

(11) Nagaoka, K.; Naruse, H.; Shinohara, I.; Watanabe, M. High ionic conductivity in poly(dimethyl siloxane-co-ethylene oxide) dissolving lithium perchlorate. *J. Polym. Sci., Polym. Lett. Ed.* **1984**, *22*, 659−663.

(12) Nishimoto, A.; Watanabe, M.; Ikeda, Y.; Kohjiya, S. High ionic conductivity of new polymer electrolytes based on high molecular weight polyether comb polymers. *Electrochim. Acta* **1998**, *43*, 1177−1184.

(13) Watanabe, M.; Endo, T.; Nishimoto, A.; Miura, K.; Yanagida, M. High ionic conductivity and electrode interface properties of polymer electrolytes based on high molecular weight branched polyether. *J. Power Sources* **1999**, *81*−*82*, 786−789.

(14) Nishimoto, A.; Agehara, K.; Furuya, N.; Watanabe, T.; Watanabe, M. High Ionic Conductivity of Polyether-Based Network Polymer Electrolytes with Hyperbranched Side Chains. *Macromolecules* **1999**, *32*, 1541−1548.

(15) Acosta, J. Structural, morphological and electrical characterization of polymer electrolytes based on PEO/PPO blends. *Solid State Ionics* **1996**, *85*, 85−90.

(16) Zhang, Z.; Jin, J.; Bautista, F.; Lyons, L.; Shariatzadeh, N.; Sherlock, D.; Amine, K.; West, R. Ion conductive characteristics of cross-linked network polysiloxane-based solid polymer electrolytes. *Solid State Ionics* **2004**, *170*, 233−238.

(17) Watanabe, M. Polymer electrolytes derived from dendritic polyether macromonomers. *Solid State Ionics* **2002**, *148*, 399−404.

(18) Croce, F.; Persi, L.; Scrosati, B.; Serraino-Fiory, F.; Plichta, E.; Hendrickson, M. A. Role of the ceramic fillers in enhancing the transport properties of composite polymer electrolytes. *Electrochim. Acta* **2001**, *46*, 2457−2461.

(19) Johansson, P.; Ratner, M. A.; Shriver, D. F. The Influence of Inert Oxide Fillers on Poly(ethylene oxide) and Amorphous Poly(ethylene oxide) Based Polymer Electrolytes. *J. Phys. Chem. B* **2001**, *105*, 9016−9021.

DOI: 10.1021/acs.macromol.7b02706
Macromolecules 2018, 51, 2847−2858

(20) Baldwin, K. R.; Golder, A. J.; Knight, J. Polymer Electrolytes: An Investigation of Some Poly (N-Propylaziridine)/Lithium Salt Compositions, 1984.
(21) Harris, C. S.; Shriver, D. F.; Ratner, M. A. Complex formation of polyethylenimine with sodium triflate and conductivity behavior of the complexes. *Macromolecules* **1986**, *19*, 987−989.
(22) Morioka, T.; Ota, K.; Tominaga, Y. Effect of oxyethylene side chains on ion-conductive properties of polycarbonate-based electrolytes. *Polymer* **2016**, *84*, 21−26.
(23) Smith, M.; Silva, M.; Cerqueira, S.; MacCallum, J. R. Preparation and characterization of a lithium ion conducting electrolyte based on poly(trimethylene carbonate). *Solid State Ionics* **2001**, *140*, 345−351.
(24) Armstrong, R. D.; Clarke, M. D. Lithium ion conducting polymeric electrolytes based on poly(ethylene adipate). *Electrochim. Acta* **1984**, *29*, 1443−1446.
(25) Dupon, R. Ion Transport in the Polymer Electrolytes Formed Between Poly(ethylene succinate) and Lithium Tetrafluoroborate. *J. Electrochem. Soc.* **1984**, *131*, 586−589.
(26) Watanabe, M.; Togo, M.; Sanui, K.; Ogata, N.; Kobayashi, T.; Ohtaki, Z. Ionic conductivity of polymer complexes formed by poly(β-propiolactone) and lithium perchlorate. *Macromolecules* **1984**, *17*, 2908−2912.
(27) Watanabe, M.; Rikukawa, M.; Sanui, K.; Ogata, N.; Kato, H.; Kobayashi, T.; Ohtaki, Z. Ionic conductivity of polymer complexes formed by poly(ethylene succinate) and lithium perchlorate. *Macromolecules* **1984**, *17*, 2902−2908.
(28) Lee, Y.-C.; Ratner, M. A.; Shriver, D. F. Ionic conductivity in the poly(ethylene malonate)/lithium triflate system. *Solid State Ionics* **2001**, *138*, 273−276.
(29) Barteau, K. P.; Wolffs, M.; Lynd, N. A.; Fredrickson, G. H.; Kramer, E. J.; Hawker, C. J. Allyl Glycidyl Ether-Based Polymer Electrolytes for Room Temperature Lithium Batteries. *Macromolecules* **2013**, *46*, 8988−8994.
(30) Cowie, J. M. G.; Martin, A. C. S. Ionic conductivity in poly(di-poly(propylene glycol) itaconate)-salt mixtures. *Polymer* **1987**, *28*, 627−632.
(31) Blonsky, P.; Shriver, D.; Austin, P.; Allcock, H. Complex formation and ionic conductivity of polyphosphazene solid electrolytes. *Solid State Ionics* **1986**, *18−19*, 258−264.
(32) Hooper, R.; Lyons, L. J.; Moline, D. A.; West, R. A Highly Conductive Solid-State Polymer Electrolyte Based on a Double-Comb Polysiloxane Polymer with Oligo(ethylene oxide) Side Chains. *Organometallics* **1999**, *18*, 3249−3251.
(33) Hooper, R.; Lyons, L. J.; Mapes, M. K.; Schumacher, D.; Moline, D. A.; West, R. Highly Conductive Siloxane Polymers. *Macromolecules* **2001**, *34*, 931−936.
(34) Watanabe, M.; Nagano, S.; Sanui, K.; Ogata, N. Ion conduction mechanism in network polymers from poly(ethylene oxide) and poly(propylene oxide) containing lithium perchlorate. *Solid State Ionics* **1986**, *18−19*, 338−342.
(35) Sarapas, J. M.; Tew, G. N. Poly(ether−thioethers) by Thiol−Ene Click and Their Oxidized Analogues as Lithium Polymer Electrolytes. *Macromolecules* **2016**, *49*, 1154−1162.
(36) Matoba, Y. Ionic conductivity and mechanical properties of polymer networks prepared from high molecular weight branched poly(oxyethylene)s. *Solid State Ionics* **2002**, *147*, 403−409.
(37) Choi, B. K.; Kim, Y. W.; Shin, H. K. Ionic conduction in PEO-PAN blend polymer electrolytes. *Electrochim. Acta* **2000**, *45*, 1371−1374.
(38) Newman, J.; Thomas-Alyea, K. E. *Electrochemical Systems*; John Wiley & Sons: 2012; Vol. *27*.
(39) Bruce, P. G.; Vincent, C. A. Steady state current flow in solid binary electrolyte cells. *J. Electroanal. Chem. Interfacial Electrochem.* **1987**, *225*, 1−17.
(40) Evans, J.; Vincent, C. A.; Bruce, P. G. Electrochemical measurement of transference numbers in polymer electrolytes. *Polymer* **1987**, *28*, 2324−2328.
(41) Balsara, N. P.; Newman, J. Relationship between Steady-State Current in Symmetric Cells and Transference Number of Electrolytes Comprising Univalent and Multivalent Ions. *J. Electrochem. Soc.* **2015**, *162*, A2720−A2722.
(42) Pesko, D. M.; Timachova, K.; Bhattacharya, R.; Smith, M. C.; Villaluenga, I.; Newman, J.; Balsara, N. P. Negative Transference Numbers in Poly(ethylene oxide)-Based Electrolytes. *J. Electrochem. Soc.* **2017**, *164*, E3569−E3575.
(43) Doyle, M.; Newman, J. Analysis of Transference Number Measurements Based on the Potentiostatic Polarization of Solid Polymer Electrolytes. *J. Electrochem. Soc.* **1995**, *142*, 3465.
(44) Chintapalli, M.; Timachova, K.; Olson, K. R.; Mecham, S. J.; Devaux, D.; DeSimone, J. M.; Balsara, N. P. Relationship between Conductivity, Ion Diffusion, and Transference Number in Perfluoropolyether Electrolytes. *Macromolecules* **2016**, *49*, 3508−3515.
(45) Jo, G.; Jeon, H.; Park, M. J. Synthesis of Polymer Electrolytes Based on Poly(ethylene oxide) and an Anion-Stabilizing Hard Polymer for Enhancing Conductivity and Cation Transport. *ACS Macro Lett.* **2015**, *4*, 225−230.
(46) Watanabe, M.; Nagano, S.; Sanui, K.; Ogata, N. Estimation of Li + transport number in polymer electrolytes by the combination of complex impedance and potentiostatic polarization measurements. *Solid State Ionics* **1988**, *28-30*, 911−917.
(47) Kato, Y.; Watanabe, M.; Sanui, K.; Ogata, N. Ionic transport number of network PEO electrolytes. *Solid State Ionics* **1990**, *40-41*, 632−636.
(48) Tominaga, Y.; Yamazaki, K. Fast Li-ion conduction in poly(ethylene carbonate)-based electrolytes and composites filled with TiO_2 nanoparticles. *Chem. Commun.* **2014**, *50*, 4448.
(49) Tominaga, Y.; Yamazaki, K.; Nanthana, V. Effect of Anions on Lithium Ion Conduction in Poly(ethylene carbonate)-based Polymer Electrolytes. *J. Electrochem. Soc.* **2015**, *162*, A3133−A3136.
(50) Geiculescu, O. E.; Rajagopal, R.; Creager, S. E.; DesMarteau, D. D.; Zhang, X.; Fedkiw, P. Transport Properties of Solid Polymer Electrolytes Prepared from Oligomeric Fluorosulfonimide Lithium Salts Dissolved in High Molecular Weight Poly(ethylene oxide). *J. Phys. Chem. B* **2006**, *110*, 23130−23135.
(51) Nekoomanesh, H. M.; Nagae, S.; Booth, C.; Owen, J. R. The Effect of Oxyethylene Sequence Length on the Properties of Poly[oxymethylene-oligo(oxyethylene)]/LiClO[sub 4] Polymer Electrolytes. *J. Electrochem. Soc.* **1992**, *139*, 3046.
(52) Nagae, S.; Nekoomanesh, H. M.; Booth, C.; Owen, J. R. The effect of salt concentration on the properties of poly[oxymethylene-oligo (oxyethylene)]/LiClO4 polymer electrolytes. *Solid State Ionics* **1992**, *53−56*, 1118−1124.
(53) Sloop, S. E.; Lerner, M. M. Study of the Poly[oxymethylene oligo-(oxyethylene)]/Lithium Metal Interface. *J. Electrochem. Soc.* **1996**, *143*, 1292.
(54) Nicholas, C. V.; Wilson, D. J.; Booth, C.; Giles, J. R. M. Improved synthesis of oxymethylene-linked poly(oxyethylene). *Br. Polym. J.* **1988**, *20*, 289−292.
(55) Linden, E.; Owen, J. R. Conductivity measurements on amorphous PEO copolymers. *Solid State Ionics* **1988**, *28−30*, 994−1000.
(56) Xu, B.; Lillya, C. P.; Chien, J. C. W. Cationic Polymerizations of 1,3,6-Trioxocane and 2-Butyl-1,3,6-trioxocane. *Macromolecules* **1987**, *20*, 1445−1450.
(57) Okada, M.; Kozawa, S.; Yamashita, Y. Kinetic studies on the polymerization of 1.3.6-trioxocane catalyzed by triethyl oxonium tetrafluoroborate. *Makromol. Chem.* **1969**, *127*, 66−77.
(58) Kawakami, Y.; Yamashita, Y. Macrocyclic Formals. 3. Two-Stage Polymerization of 1,3-Dioxacycloalkanes. *Macromolecules* **1977**, *10*, 837−839.
(59) Teran, A. A.; Tang, M. H.; Mullin, S. A.; Balsara, N. P. Effect of molecular weight on conductivity of polymer electrolytes. *Solid State Ionics* **2011**, *203*, 18−21.
(60) Devaux, D.; Bouchet, R.; Glé, D.; Denoyel, R. Mechanism of ion transport in PEO/LiTFSI complexes: Effect of temperature, molecular weight and end groups. *Solid State Ionics* **2012**, *227*, 119−127.
(61) Shi, J.; Vincent, C. The effect of molecular weight on cation mobility in polymer electrolytes. *Solid State Ionics* **1993**, *60*, 11−17.

DOI: 10.1021/acs.macromol.7b02706
Macromolecules 2018, 51, 2847−2858

(62) Plimpton, S. Fast Parallel Algorithms for Short-Range Molecular-Dynamics. *J. Comput. Phys.* **1995**, *117*, 1−19.
(63) Webb, M. A.; Savoie, B. M.; Wang, Z.-G.; Miller, T. F., III Chemically Specific Dynamic Bond Percolation Model for Ion Transport in Polymer Electrolytes. *Macromolecules* **2015**, *48*, 7346−7358.
(64) Alves, N. M.; Mano, J. F.; Balaguer, E.; Meseguer Dueñas, J. M.; Gómez Ribelles, J. L. Glass transition and structural relaxation in semi-crystalline poly(ethylene terephthalate): A DSC study. *Polymer* **2002**, *43*, 4111−4122.
(65) Mano, J. F.; Gómez Ribelles, J. L.; Alves, N. M.; Salmerón Sanchez, M. Glass transition dynamics and structural relaxation of PLLA studied by DSC: Influence of crystallinity. *Polymer* **2005**, *46*, 8258.
(66) Liu, G.; Reeder, C. L.; Sun, X.; Kerr, J. B. Diffusion coefficients in trimethyleneoxide containing comb branch polymer electrolytes. *Solid State Ionics* **2004**, *175*, 781−783.
(67) Killis, A.; LeNest, J.; Cheradame, H.; Gandini, A. Ionic conductivity of polyether-polyurethane networks containing NaBPh4: A free volume analysis. *Makromol. Chem.* **1982**, *183*, 2835−2845.
(68) Lascaud, S.; Perrier, M.; Vallee, A.; Besner, S.; Prud'homme, J.; Armand, M. Phase Diagrams and Conductivity Behavior of Poly-(ethylene oxide)-Molten Salt Rubbery Electrolytes. *Macromolecules* **1994**, *27*, 7469−7477.
(69) Armand, M. B.; Chabagno, J. M.; Duclot, M. J. Poly-ethers as solid electrolytes. In *Fast Ion Transport in Solids*; Vashishta, P. M., Mundy, J. N., Shenoy, G. K., Eds.; North-Holland: 1979; pp 131−136.
(70) MacCallum, J. R.; Vincent, C. A. *Polymer Electrolyte Reviews*; Springer Science & Business Media: 1987; Vol. *1*.
(71) Ratner, M. A.; Shriver, D. F. Ion transport in solvent-free polymers. *Chem. Rev.* **1988**, *88*, 109−124.
(72) Pesko, D. M.; Jung, Y.; Hasan, A. L.; Webb, M. A.; Coates, G. W.; Miller, T. F., III; Balsara, N. P. Effect of monomer structure on ionic conductivity in a systematic set of polyester electrolytes. *Solid State Ionics* **2016**, *289*, 118−124.
(73) Bhattacharja, S.; Smoot, S.; Whitmore, D. Cation and anion diffusion in the amorphous phase of the polymer electrolyte (PEO) 8LiCF3SO3. *Solid State Ionics* **1986**, *18−19*, 306−314.
(74) Hafezi, H.; Newman, J. Verification and Analysis of Transference Number Measurements by the Galvanostatic Polarization Method. *J. Electrochem. Soc.* **2000**, *147*, 3036.
(75) Orädd, G.; Edman, L.; Ferry, A. Diffusion: a comparison between liquid and solid polymer LiTFSI electrolytes. *Solid State Ionics* **2002**, *152-153*, 131−136.
(76) Timachova, K.; Watanabe, H.; Balsara, N. P. Effect of Molecular Weight and Salt Concentration on Ion Transport and the Transference Number in Polymer Electrolytes. *Macromolecules* **2015**, *48*, 7882−7888.
(77) Gorecki, W.; Jeannin, M.; Belorizky, E.; Roux, C.; Armand, M. Physical properties of solid polymer electrolyte PEO(LiTFSI) complexes. *J. Phys.: Condens. Matter* **1995**, *7*, 6823−6832.
(78) Pożyczka, K.; Marzantowicz, M.; Dygas, J. R.; Krok, F. Ionic Conductivity and Lithium Transference Number of Poly(Ethylene Oxide):LiTFSI System. *Electrochim. Acta* **2017**, *227*, 127−135.
(79) Shah, D. B.; Olson, K. R.; Karny, A.; Mecham, S. J.; DeSimone, J. M.; Balsara, N. P. Effect of Anion Size on Conductivity and Transference Number of Perfluoroether Electrolytes with Lithium Salts. *J. Electrochem. Soc.* **2017**, *164*, A3511−A3517.
(80) Webb, M. A.; Jung, Y.; Pesko, D. M.; Savoie, B. M.; Yamamoto, U.; Coates, G. W.; Balsara, N. P.; Wang, Z.-G.; Miller, T. F. Systematic Computational and Experimental Investigation of Lithium-Ion Transport Mechanisms in Polyester-Based Polymer Electrolytes. *ACS Cent. Sci.* **2015**, *1*, 198−205.

DOI: 10.1021/acs.macromol.7b02706
Macromolecules 2018, 51, 2847−2858